

The *BABAR* Electromagnetic Calorimeter: Status and Performance Improvements

Johannes M. Bauer
for the EMC Group of the *BABAR* Collaboration

Abstract

The electromagnetic calorimeter at the *BABAR* detector, part of the asymmetric B Factory at SLAC, measures photons in the energy range from 20 MeV to 8 GeV with high resolution. The current status of the calorimeter, now in its seventh year of operation, is being presented, as well as details on improvements made to the analysis code during the last years.

Submitted to the Conference Proceedings of the IEEE Nuclear Science Symposium
and Medical Imaging Conference, October 23 – 29, 2005, Puerto Rico, U.S.A.

Stanford Linear Accelerator Center, Stanford University, Stanford, CA 94309

Work supported in part by Department of Energy contract DE-AC02-76SF00515
and Department of Energy grant DE-FG05-91ER40622.

The *BABAR* Electromagnetic Calorimeter: Status and Performance Improvements

Johannes M. Bauer, *Member, IEEE, for the EMC Group of the BABAR Collaboration*

Abstract—The electromagnetic calorimeter at the *BABAR* detector, part of the asymmetric B Factory at SLAC, measures photons in the energy range from 20 MeV to 8 GeV with high resolution. The current status of the calorimeter, now in its seventh year of operation, is being presented, as well as details on improvements made to the analysis code during the last years.

Index Terms—*BABAR*, calorimeter, CsI(Tl), calibration, Bhabha, neutron sources, radiation damage.

I. THE SLAC B-FACILITY

SINCE 1999, the asymmetric B factory at the Stanford Linear Accelerator Center (SLAC) is colliding 9.0 GeV electrons with 3.1 GeV positrons. This total energy of 10.58 GeV corresponds to the $\Upsilon(4S)$ resonance. Its decay particles, B^+B^- and $B^0\bar{B}^0$ pairs, are used to study CP violation and many other processes in particle physics. The data are collected by the *BABAR* Detector (Figs. 1 and 2), which is described in detail in Ref. [1].

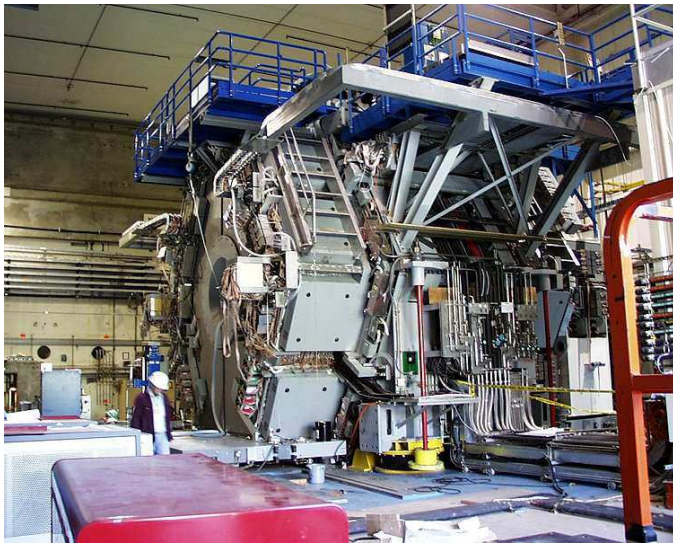


Fig. 1. The *BABAR* detector during the time of construction.

II. ELECTROMAGNETIC CALORIMETER OVERVIEW

The electromagnetic calorimeter (EMC) consists of 6580 CsI(Tl) crystals 16 to 17.5 radiation lengths deep (Fig. 3 left),

Manuscript received November 18, 2005. This work was supported by U.S. Department of Energy grant DE-FG05-91ER40622.

J.M. Bauer is with the University of Mississippi.

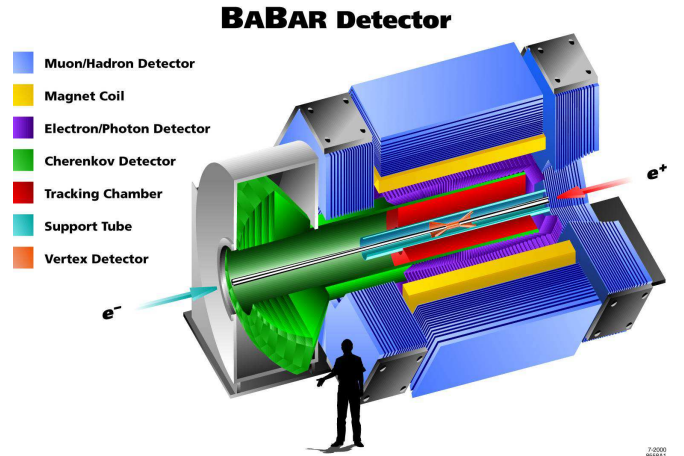


Fig. 2. Schematic drawing of the *BABAR* detector. The electromagnetic calorimeter is the subsystem shown in purple.

all pointing close to the interaction point. At the back of each crystal two photo diodes and one pre-amplifier card are attached (Fig. 3 right). On average, the diodes see about 7,300 photo-electrons/MeV. The electronics covers the signal with an 18-bit dynamic range by combining the output of a 10-bit ADC with two range bits. This allows the calorimeter to measure photon energies from 20 MeV to 8 GeV. The energy and position resolution was determined to be the following [2]:

$$\frac{\sigma_E}{E} = \frac{(2.30 \pm 0.03 \pm 0.3)\%}{\sqrt[4]{E(\text{GeV})}} \oplus (1.35 \pm 0.08 \pm 0.2)\% \quad (1)$$

$$\sigma_\theta = \sigma_\phi = \frac{(4.16 \pm 0.04) \text{ mrad}}{\sqrt{E(\text{GeV})}} \quad (2)$$

The crystals are combined into 7×3 modules (except for 6×3 modules at the backward end and special modules for the forward end), then assembled like shown in Figure 4 into a barrel and an endcap. Fig. 5 gives a view inside the barrel during assembly, while in Fig. 6 the completed barrel is waiting for its insertion into the detector.

III. PERFORMANCE OF HARDWARE

The operation of the calorimeter is very stable. Out of 6580 crystals, only one crystal is dead with no hope for any recovery. Currently four more crystals are dead, but they might be recovered at some time. Fourteen more crystals use only one of the two diodes; several more crystals are working incorrectly in one energy range, for example at low energy. From time

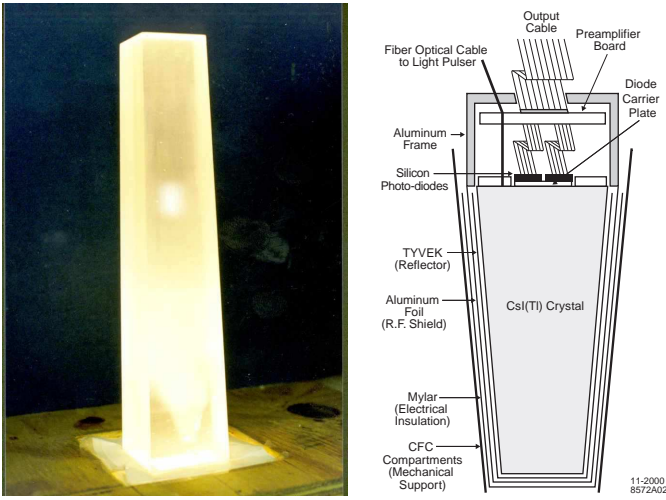


Fig. 3. Left: Photograph of a CsI(Tl) crystal lit from the bottom by a light bulb. Right: Schematic drawing (not to scale) of a crystal with attached electronics.

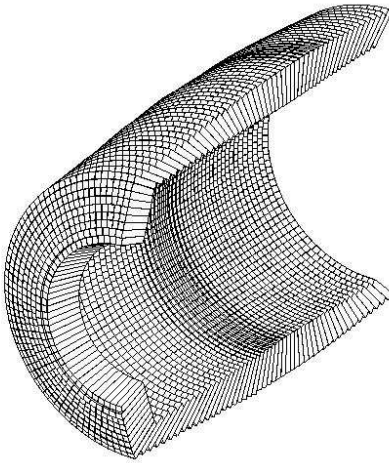


Fig. 4. Cutout drawing of the cylindrical arrangement of the crystals into the large barrel and the smaller endcap (left bottom).

to time an ADC board becomes noisy, which, in the worst case, results in the crystals of this board being masked out until the board can be replaced during the next access to the detector. The electronics is regularly calibrated by determining the pedestals and by injecting a known charge into the pre-amplifiers to measure the gain and linearity of the system (see also Ref. [3]).

IV. CALIBRATION OF INDIVIDUAL CRYSTALS

The individual response of a crystal to deposited energy, namely its overall light yield and its non-uniformity in the light output (the dependence on the location of the shower inside the crystal), depends on the details at time of manufacture and the shape of the crystal. The light output also decreases over time due to radiation damage. Each crystal of the *BABAR* calorimeter is therefore regularly calibrated. Two absolute energy calibrations are employed for this: The liquid source calibration at low energy and the Bhabha calibration at high

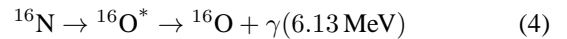
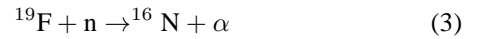


Fig. 5. Photograph of the inside of the barrel calorimeter during construction.

energy. For intermediate energies the calibration constants are interpolations between these two extremes following a function linear in the logarithm of the energy.

A. Liquid Source System

Whenever a liquid source calibration is performed, a neutron generator is switched on to emit 14 MeV neutrons. The generator is surrounded by Fluorinert (FC77), a liquid rich in fluorine, and the following chain results in the emission of 6.13 MeV photons through the decay of ^{16}N with a half-life time of 7 seconds:



A system of pipes transports the radioactive liquid past the front of the crystals. There the photons enter the crystals and are detected with the regular data acquisition system. Figure 7 shows the spectrum of these photons as seen by a crystal in the

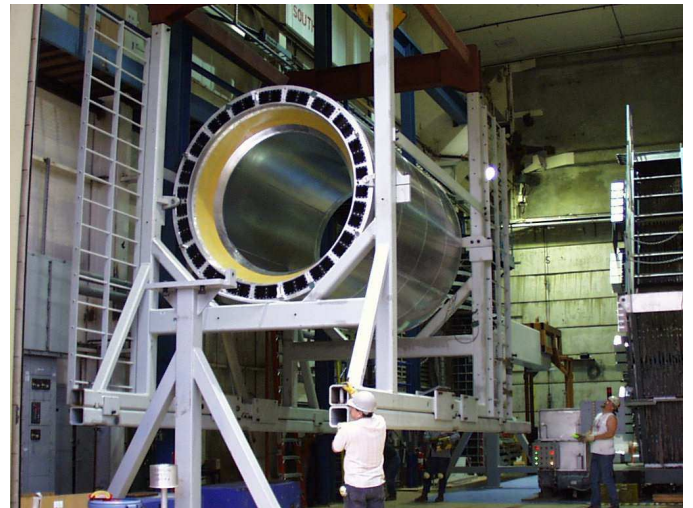


Fig. 6. Completed barrel calorimeter ready for installation in the detector.

calorimeter. Calibrations are performed about once a month to a statistical uncertainty of $\leq 0.5\%$ and a systematic uncertainty of about 0.1% . The average loss in light yield over time due to radiation damage as measured by the liquid source system is documented in Fig. 8. Radiation measurements by RadFETs located at the calorimeter indicate that the average radiation dose so far is ~ 0.7 kRad for the barrel and ~ 1.1 kRad for the endcap [4] [5]. For more details on the liquid source calibration system see Ref. [6].

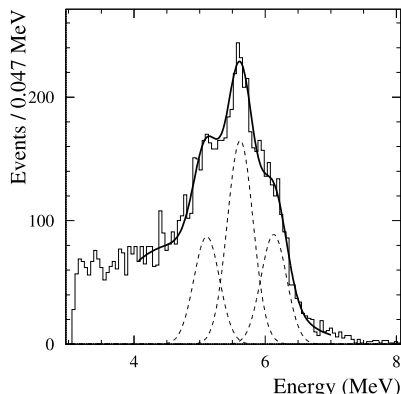


Fig. 7. Spectrum of 6.13 MeV photons as detected by a crystal of the calorimeter. The Gaussian functions indicate the contributions from the 6.13 MeV peak (far right) and the two escape peaks (middle and left).

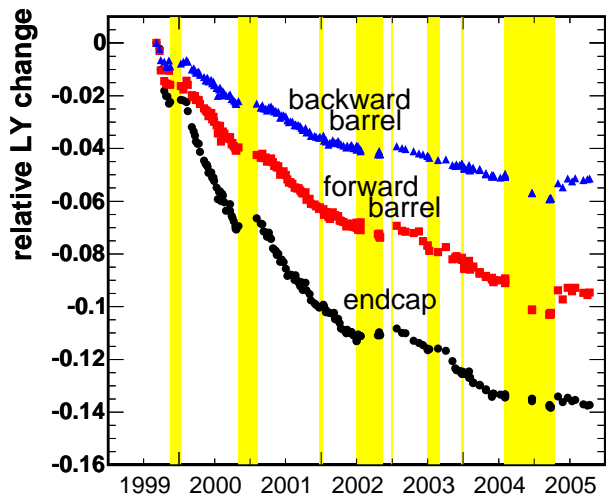


Fig. 8. Relative loss in light yield over time for the backward barrel (blue), forward barrel (red) and endcap (black) as measured by the liquid source system. The yellow areas indicate major times without beam.

B. Bhabha Calibration

The second absolute energy calibration of individual crystals is performed with $e^+e^- \rightarrow e^+e^-$ events from regular recorded data. These calibrations involve crystal energies of 2.5 GeV to 8 GeV, depending on the polar angle due to the asymmetry in the beam energies. The calibration requires most crystals to have at least 200 direct hits in order to reach a statistical error of 0.35% for individual crystals. The systematic error is estimated

to be less than 1% [7]. Calibration constants are currently calculated up to once a month, but will soon be obtained more frequently once the code is running automatically as part of the regular reconstruction system. The constants change over time in a way similar to the source calibration constants (Fig. 9).

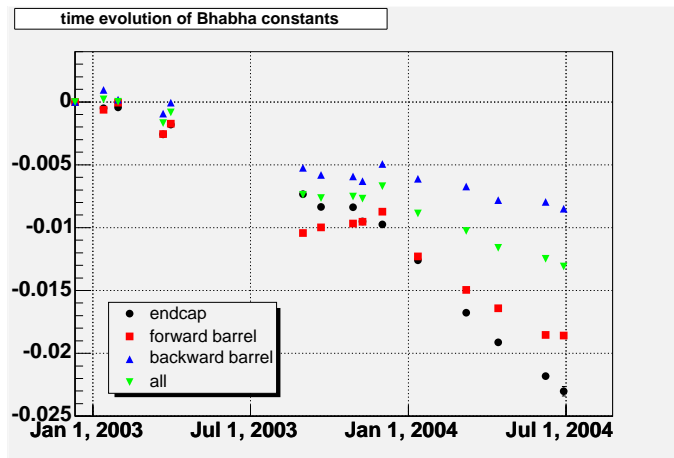


Fig. 9. Evolution of average Bhabha constants over time.

V. CLUSTER CALIBRATIONS

Not only calibrations of individual crystals are needed, but also calibrations of the clusters, which are groups of adjacent crystals in which the full shower energy of a particle is deposited. These corrections adjust for shower energy lost at the rear of the crystals, gaps between the crystals, and the sides of the calorimeter.

For clusters with energies up to 2 GeV, the calibration is obtained from π^0 mesons by correcting the photon energies so that the distribution of the invariant mass of two photons agrees with the expected π^0 mass distribution. Corrections are mostly in the 6% to 8% range. Figure 10 shows a typical $m(\gamma\gamma)$ distribution with a clear π^0 peak. An improved version of the calibration is currently being tested.

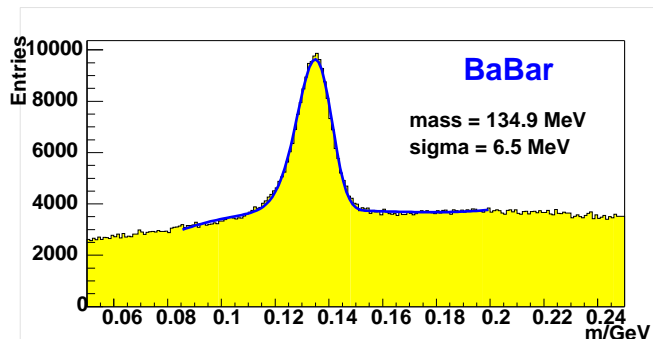


Fig. 10. Distribution of the invariant mass of photon pairs after applying the cluster calibration.

For clusters with energies above 2 GeV, the correction factors are obtained from single-photon Monte Carlo simulation. Soon new calibration constants based on $e^+e^- \rightarrow \mu\mu\gamma$ events will be introduced.

VI. IMPROVEMENTS IN RECONSTRUCTION SOFTWARE

A. Position of Cluster Inside Crystals

When matching a track to a cluster of the calorimeter, the position of the cluster in three dimensions has to be known. Until recently, this position of the cluster center was always located at the front of the crystals. This caused less than optimal performance of the matching algorithm, such as when a low-energy track, spiraling in the magnetic field of the detector, enters the calorimeter at an angle. Now all clusters are assumed to be located at a depth of 12.5 cm inside the crystals. Figure 11 displays the improvement in the matching by showing the azimuthal angle difference of the matched tracks and clusters before and after this change. Similarly, the track-matching efficiency improved, especially at very low momentum (Fig. 12).

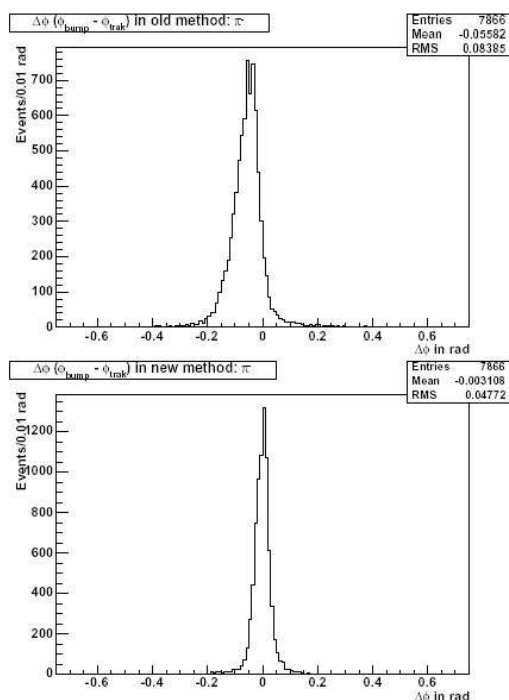


Fig. 11. Distribution of the azimuthal angle difference (in rad) of the cluster position and the point where the track intersects with the calorimeter. The plots are based on actual data with requirements applied that select a clean set of π mesons. For the top plot the old, for the bottom plot the new cluster position algorithm is used.

B. Edge Correction

If a photon hits the calorimeter at a position close to the edge between two crystals, up to 3% of its energy is lost in gaps, as can be seen from Figs. 13 and 14. A correction is now applied to the energy of each cluster. The effect of this so-called “edge correction” on physics analyses can be seen from the distributions in Fig. 15. The quantity plotted is ΔE , the difference between the measured energy of a B meson candidate minus the known beam energy. Without measurement uncertainties, the peak would be exactly at zero. The underlying

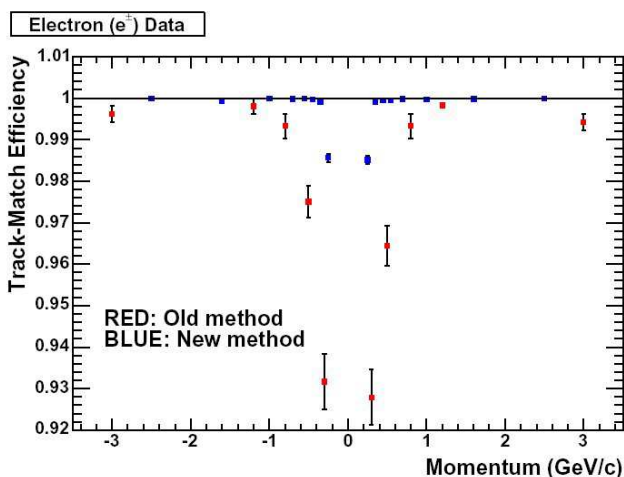


Fig. 12. Track matching efficiency versus momentum for electrons and positrons. The plot is based on actual data with requirements that select a clean set of electrons and positrons. For the points in red the old, for the points in blue the new cluster position algorithm is used.

data set of the shown distributions is Monte Carlo simulation of the decay $B^+ \rightarrow K^{*+}\gamma$. The left plot, obtained without edge correction, has a FWHM/2.36 of (45.1 ± 0.7) MeV, while the right plot, obtained with edge correction, has a FWHM/2.36 of (42.0 ± 0.6) MeV, which means that in this case the edge correction improved the ΔE resolution by 7%.

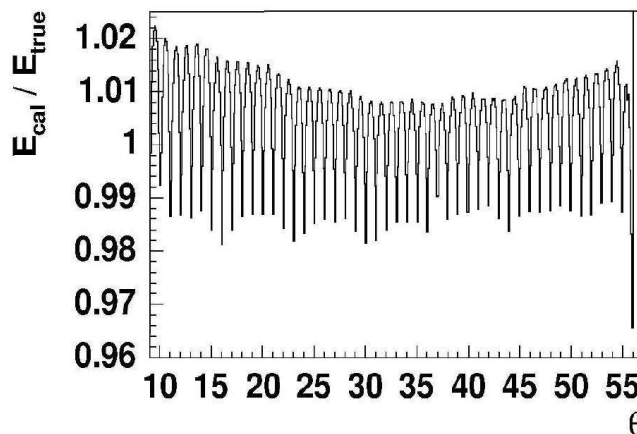


Fig. 13. Ratio of reconstructed over true energy of photons versus crystal ring of the barrel. The forward end (where the endcap is attached) is on the left side, the backward end on the right side. The plot is based on $B\bar{B}$ Monte Carlo simulation with measured photon energy E_{cal} between 0.5 GeV and 0.8 GeV.

VII. ADDITIONAL STUDIES AND FUTURE GOALS

Many decay modes are being used to study the performance of the calorimeter, like $e^+e^- \rightarrow \mu\mu\gamma$ events, radiative Bhabha events ($e^+e^- \rightarrow e^+e^-\gamma$), $e^+e^- \rightarrow \gamma\gamma$, $D^{*0} \rightarrow D^0\gamma$ (photon energies from 100 to 400 MeV), $\Sigma_0 \rightarrow \Lambda\gamma$ (photon energies from 50 to 250 MeV). A new cluster calibration is about to be implemented, and the Bhabha calibration will soon be automated to provide more frequent monitoring and correction of the radiation damage at high energies.

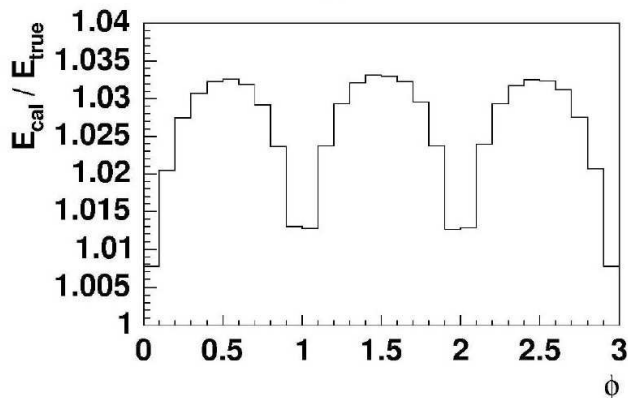


Fig. 14. Ratio of reconstructed over true energy of photons versus azimuthal angle in units of crystals. Due to the modular structure in the calorimeter, the crystals are folded over into one single group of three crystals. The dips at 0 and 3 are deeper because of the larger gap between the crystal modules. The plot is based on $B\bar{B}$ Monte Carlo simulation with measured photon energy E_{cal} between 0.5 GeV and 0.8 GeV.

VIII. CONCLUSION

The *BABAR* electromagnetic calorimeter operates very reliably and delivers very good performance for the experiment. The damage to the crystals due to radiation is regularly measured and calibrated out. Over time, enhancements were added to the reconstruction code, and the tweaking of the calibrations continues in order to improve the reconstruction of the detected particles and ultimately improve the physics analyses of *BABAR*.

ACKNOWLEDGMENT

The author thanks everyone in the *BABAR* EMC group for all their contributions to the calorimeter. He congratulates and extends his gratitude to the whole *BABAR* Collaboration and the PEP-II accelerator group for their tremendous accomplishments.

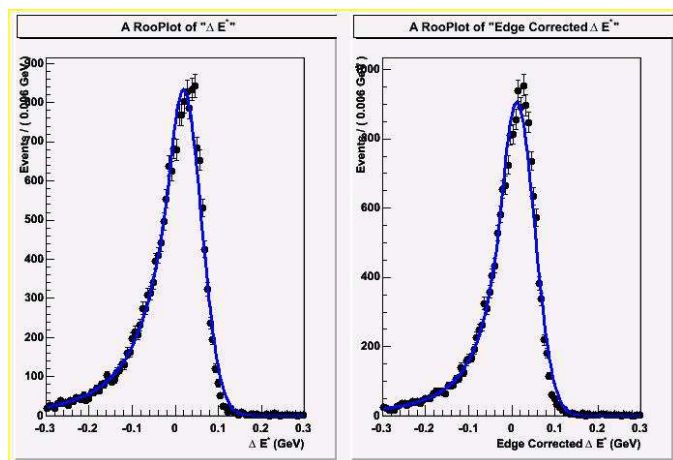


Fig. 15. Distribution of the quantity ΔE for signal Monte Carlo events $B^+ \rightarrow K^{*+}\gamma$. The left plot was obtained without, the right plot with the edge correction.

REFERENCES

- [1] *BABAR* Collaboration, B. Aubert, A. Bazan, A. Boucham, D. Boutigny, I. De Bonis, J. Favier *et al.*, “The *BABAR* detector,” *Nucl. Instrum. Methods*, vol. A479, pp. 1–116, Feb./Mar. 2002.
- [2] M. Kocian, “Performance and calibration of the crystal calorimeter of the *BABAR* detector,” in *Proc. 10th Int. Conf. Calorimetry in Particle Physics (CALOR 2002)*, Pasadena, CA, Mar. 2002, pp. 167–174.
- [3] I. G. Eschrich, “The *BABAR* electromagnetic calorimeter in its third year of operation,” in *Proc. 10th Int. Conf. Calorimetry in Particle Physics (CALOR 2002)*, Pasadena, CA, Mar. 2002, pp. 658–664.
- [4] B. Camanzi, H. B. Crawley, A. Holmes-Siedle, R. L. McKay, A. McKemey, W. T. Meyer *et al.*, “The *BABAR* RadFET monitoring board,” *IEEE Trans. Nucl. Sci.*, vol. 49, pp. 1275–1280, June 2002.
- [5] A. Khan, T. Meyer, J. Stelzer, and J. Yi, “The radiation dose measurement system for the *BABAR* electromagnetic calorimeter,” this conference record.
- [6] J. M. Bauer, “Absolute energy calibration with the neutron-activated liquid-source system at *BABAR*’s CsI(Tl) calorimeter,” *IEEE Trans. Nucl. Sci.*, vol. 51, pp. 1596–1600, Aug. 2004.
- [7] R. Müller-Pfefferkorn, “Die Kalibration des elektromagnetischen CsI(Tl)-Kalorimeters des *BABAR*-Detektors mit Ereignissen der Bhabha-Streuung,” dissertation (in German), Technische Universität Dresden (2001), *BABAR-THESIS-01/004*.